ARTICLE **OPEN**

Check for updates

Process optimization of osmotic membrane distillation for the extraction of valuable resources from water streams

Matteo Morciano [1,2,4], Marco Malaguti [3,4], Francesco Ricceri[2,3], Alberto Tiraferri [2,3 ✉] and Matteo Fasano [1,2 ✉]

The rising demand for sustainable wastewater management and high-value resource recovery is pressing industries involved in, e.g., textiles, metals, and food production, to adopt energy-efficient and flexible liquid separation methods. The current techniques often fall short in achieving zero liquid discharge and enhancing socio-economic growth sustainably. Osmotic membrane distillation (OMD) has emerged as a low-temperature separation process designed to concentrate valuable elements and substances in dilute feed streams. The efficacy of OMD hinges on the solvent's migration from the feed to the draw stream through a hydrophobic membrane, driven by the vapor pressure difference induced by both temperature and concentration gradients. However, the intricate interplay of heat and mass processes steering this mechanism is not yet fully comprehended or accurately modeled. In this research, we conducted a combined theoretical and experimental study to explore the capabilities and thermodynamic limitations of OMD. Under diverse operating conditions, the experimental campaign aimed to corroborate our theoretical assertions. We derived a novel equation to govern water flux based on foundational principles and introduced a streamlined version for more straightforward application. Our findings spotlight complex transport-limiting and self-adjusting mechanisms linked with temperature and concentration polarization phenomena. Compared with traditional methods like membrane distillation and osmotic dilution, which are driven by solely temperature or concentration gradients, OMD may provide improved and flexible performance in target applications. For instance, we show that OMD—if properly optimized—can achieve water vapor fluxes 50% higher than osmotic dilution. Notably, OMD operation at reduced feed temperatures can lead to energy savings ranging between 5 and 95%, owing to the use of highly concentrated draw solutions. This study underscores the potential of OMD in real-world applications, such as concentrating lithium in wastewater streams. By enhancing our fundamental understanding of OMD's potential and constraints, we aim to broaden its adoption as a pivotal liquid separation tool, with focus on sustainable resource recovery.

INTRODUCTION

In recent years, increasingly energy-efficient techniques for water and wastewater treatment, product separation/concentration, and for valuable resource recovery from various liquid and waste streams (e.g., from textile, pharmaceutical, metallurgical, food, and beverage industries) have been receiving considerable interest to help achieving zero liquid discharge (ZLD) and sustainable socio-economic growth[1]. For instance, the demand for metals and other critical raw materials is expected to increase sharply over the coming years with developing countries experiencing substantial economic expansion. A long-term sustainable and adequate metal and mineral stock is therefore strongly required for proper techno-economic development[2]. Conventional supply relies on intensive mining, that is, an extremely costly action with impacts on ecosystems[3,4]. Furthermore, in industries such as food, beverage, nutraceuticals, and cosmetics, there is a critical need for controlled separation and concentration of various high-value and highly nutritious components, including proteins, vitamins, whey, anti-oxidants, anti-inflammatory compounds, and herbal substances[4–7]. Traditional methods employed in commercial juice treatment, for instance, often involve multi-stage vacuum evaporation at high temperature, followed by the recovery of volatile flavors, which are subsequently added to the concentrated product[8]. However, these high temperature-based techniques are not optimal at preserving the original quality of products[8–10]. Less invasive techniques that provide superior quality are, for example, cryoconcentration, an expensive (both from capital and operational cost perspectives) and energy intensive approach, as well as membrane-based processes[8].

In this rapidly evolving context, *osmotically-assisted* or "osmotic" *membrane distillation* (OMD) represents an attractive low-temperature[4,11] process by which valuable non-volatile components can be concentrated for subsequent easier recovery through solvent extraction from various dilute streams[4,12]. In the main instance of this process, an aqueous dilute feed stream (e.g., solution containing valuable materials or nutraceuticals) and a concentrated draw solution (e.g., a hypertonic salt solution) are separated by a hydrophobic and microporous membrane, which allows the flow of water vapor only. The migration of water from the feed to the draw stream is due to the vapor pressure gradient between the two sides of the membrane, and it results in increasing feed concentration while diluting the draw stream. Inorganic salts, such as sodium chloride, calcium chloride, and magnesium chloride are examples of interesting draw agents. It is worth noting that the state-of-the-art mostly includes works describing osmotic dilution/concentration processes in which the driving force is generated solely by the different activity, being the bulk temperature of the two streams equal[8,13]. However, due to

[1]Department of Energy, Politecnico di Torino, Corso Duca degli Abruzzi 24, Torino 10129, Italy. [2]CleanWaterCenter, Politecnico di Torino, Corso Duca degli Abruzzi 24, Torino 10129, Italy. [3]Department of Environment, Land and Infrastructure Engineering, Politecnico di Torino, Corso Duca degli Abruzzi 24, Torino 10129, Italy. [4]These authors contributed equally: Matteo Morciano, Marco Malaguti. ✉email: alberto.tiraferri@polito.it; matteo.fasano@polito.it

the low transmembrane fluxes observed, temperature-enhanced OMD processes have also been proposed, albeit in a limited number, where a bulk temperature difference is synergically imposed with a concentration difference, to enhance the vapor pressure gradient and thus productivity[11,14,15]. In this scenario, the bulk temperature of the feed stream, which may be heated by low-grade thermal source[11], is higher than the draw one. As flux occurs by a vapor pressure gradient across the hydrophobic membrane, one of the major strengths of OMD is the absence or the negligible presence of reverse solute diffusion to the feed stream, thus the ability to deploy highly concentrated and effective draw streams, unlike forward osmosis whereby osmotic pressure drives the flow across a hydrophilic membrane[4,13,16,17].

While OMD holds considerable promise[13,18–22], it remains insufficiently explored by the scientific community, especially concerning the fundamental transport mechanisms determining its performance. Crucially, comprehensive experimental/theoretical studies addressing the intertwined heat and mass transfer processes inherent to OMD are currently missing. Most existing models adopt a simplified approach[13,23], which, while beneficial for specific applications, inherently possesses restrictions in broader applicability. Some noteworthy works have touched upon non-equilibrium thermodynamics, polarization effects, and temperature-enhanced OMD. However, the current models often involve approximations or focus on narrow conditions, leaving a gap in understanding OMD's full potential, versatility, and intrinsic thermodynamic limitations.

Among the most relevant modeling works on OMD, Wang and co-workers[15] proposed a model based on non-equilibrium thermodynamics, neglecting the convective heat and mass transfer resistances on both sides of the membrane. Also, the model directly relates the concentration and temperature differences, which facilitates the heat and mass transfer analysis at the cost of approximations. Raghavarao and co-workers[24,25] investigated the effect of the concentration and temperature polarization on the driving force, but through a linear model and considering the activity as the only responsible variable governing the transmembrane flux. Ahmad and co-workers[26] proposed a coupled and linear heat and mass transfer model of hollow fiber membranes for salt recovery from brines via OMD, including polarization effects. Recently, Wu and co-workers[11] experimentally investigated temperature-enhanced OMD, with the feed stream heated by low-grade thermal sources (i.e., solar energy) for agricultural fertilizers. Different high-salinity solutions in the permeate or cold side were employed by the authors, namely, 1.0–4.0 M KCl solution, 3.0 M NH_4Cl solution, 3.0 M KH_2PO_4 solution, and 3.0 M urea solution. Interestingly, the analysis also involved a comparison with a more conventional process, namely, forward osmosis. The results revealed how OMD is able to guarantee comparable outlet water fluxes but negligible reverse solute flux to the feed stream[16], being therefore compatible with unconventional water streams containing various fertilizers. A similar work, authored by Zhang and co-workers[14], focused on the role of osmotic agent in water flux enhancement during temperature-enhanced osmotic membrane distillation for the treatment of highly saline brines. The authors investigated the process behavior using $MgCl_2$-based, K_2CO_3-based, and NaCl-based solutions as draw. The feed compartment was heated to always maintain an inlet temperature of 50 °C, while the permeate compartment was connected to a cooling system to maintain a constant temperature of 20 °C. Thus, the effect of different stream temperatures was not evaluated. Another important work is that discussed by Quist-Jensen and co-workers[1], where comparative experimental and theoretical analyses of membrane crystallization in direct-contact membrane distillation, OMD, and vacuum configurations were carried out with the aim to recover lithium chloride from aqueous solutions. Finally, some of the authors of this work published a recent experimental research work on the

OMD process in 2023. In detail, Tiraferri and co-workers[9] proposed using OMD for the concentration of phycocyanin and coffee extract solutions, with the goal to safeguard the quality of the extracts, using $CaCl_2$ as draw agent.

In this study, we present the development of two comprehensive models that encompass all the key phenomena involved in the conjugate heat and mass transfer mechanisms of the OMD process. Experimental campaigns, where the poorly explored[11,14,22] $CaCl_2$ is employed as draw agent, are conducted to validate the proposed modeling framework. These models, derived from fundamental principles, provide different levels of detail, accuracy, and ease of use. They are implemented to qualitatively and quantitatively investigate the influence of crucial OMD parameters, including the temperature and molarity of feed and draw solutions, on productivity (i.e., transmembrane water vapor flux) under known fluid-dynamic conditions and channel geometry. We extensively examine concentration and temperature polarization phenomena, exploring various scenarios in detail. Moreover, we provide insights into the applicability of the widely used linear model found in the literature, highlighting its strengths and limitations. Finally, we evaluate and discuss promising engineering applications in the field of valuable metal and mineral recovery, specifically focusing on lithium chloride (LiCl) concentration aimed at its extraction, considering realistic scenarios.

The overall goal of this work is to provide a validated modeling framework, at one time comprehensive and streamlined, in order to accurately and expeditiously assess the optimal operating conditions of the considered OMD process, as the application and the resources available (e.g., recoverable metal/mineral in the feed stream, draw agent, energy source) vary. The proposed model has the potential to optimize and scale up the OMD process design in diverse industries with high environmental impact.

RESULTS AND DISCUSSION

Theoretical background in brief

We developed a comprehensive modeling framework to accurately encompass all the physical mechanisms in the OMD process. This framework includes species transport, latent heat transfer resulting from phase change, heat conduction across the hydrophobic and insulating membrane, and the influences arising from the formation of temperature and concentration boundary layers at the interfaces between the aqueous solutions (both feed and draw) and the membrane (Fig. 1). Here, unlike in the classical membrane distillation process whereby freshwater typically flows in the permeate channel, the mass transport boundary layer could occur in both feed and draw channels. A counter-current direct contact configuration was considered, without losing generality. Moreover, it is worth commenting that the effect of the curvature of the liquid-vapor interface, which can be estimated using the well-known Kelvin equation, was assumed to be negligible at equilibrium, as commonly stated in the literature[27]. Extensive details on the development of the models are provided in the "Methods" section.

Modeled performance

In Fig. 2, the modeled performance of the OMD process is reported with the aim of exploring its potential and the impact of key quantities. In detail, Fig. 2a shows the water vapor flux through the membrane as predicted by the Maxwell-Stefan and dusty-gas model (see surface labeled with **I**, obtained through Eq. (4)) and by the linearized model based on Clausius-Clapeyron equation (see surface labeled with **II**, obtained through Eq. (21)), under varying values of the bulk temperature (i.e., 20 °C ≤ $T_{b,f}$ ≤ 70 °C) and molarity (0 M ≤ $c_{b,f}$ ≤ 4 M) of the feed stream. For this specific calculation, the bulk temperature and
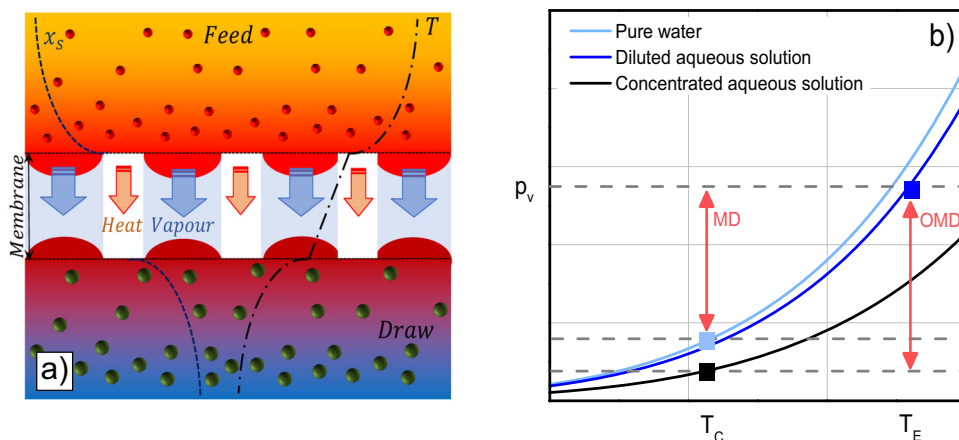
Fig. 1 Schematic diagram and working principle of counter-current direct contact osmotic membrane distillation (OMD). In (**a**), the module, which includes the feed and draw channels and the hydrophobic and porous membrane, is qualitatively represented, together with the typical temperature (T) and solute concentration (x_S) profiles as well as the resulting vapor and heat fluxes. In (**b**), vapor pressure (p_v) versus temperature (T) is reported for varying activity (a) values. The different lines refer qualitatively to freshwater (uppermost, light blue, $a = 1$), typical dilute (middle, blue, $a = 0.9$) and concentrated aqueous solutions (lowermost, black, $a = 0.5$). The double-headed arrows indicate the driving forces (i.e., the difference between the partial pressures of the feed and draw solutions) in case of classical MD and OMD. In panel **b**), the blue square qualitatively refers to thermodynamic and chemical conditions of the generic (i.e., for both MD and OMD modes) feed stream, whilst the light blue and black squares refer to thermodynamic and chemical conditions of pure water (i.e., MD mode) and concentrated draw stream (i.e., OMD mode), respectively. T_E and T_C are the evaporation and condensation temperature of the bulk fluids in the feed and draw channel, respectively.
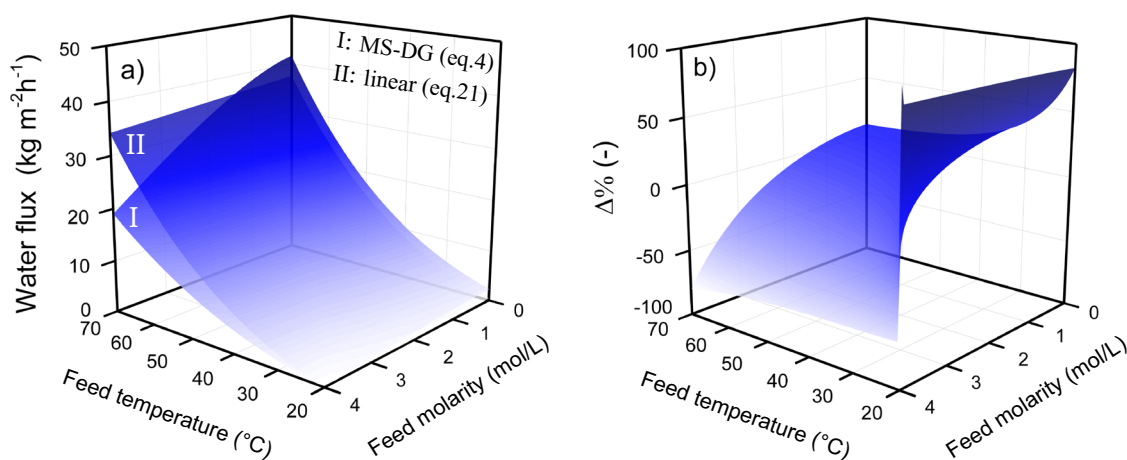

Fig. 2 Productivity of the osmotic membrane distillation process. a The steady-state specific water vapor flow rate (J_w) as a function of the bulk temperature ($T_{b,f}$) and molarity ($c_{b,f}$) of the feed stream is reported, predicted by (I) the full analytical equation, Eq. (4), and by (II) the simplified linearized version, Eq. (21). The bulk temperature and molarity of the draw stream were considered equal to 20 °C and 4 M, respectively. **b** Percent error between the two models, evaluated as $\Delta\% = \frac{J_{w,Eq.4} - J_{w,Eq.21}}{J_{w,Eq.4}}$. The membrane characteristics used for the calculations were those of the PTFE membrane deployed in the experiments.

molarity of the draw stream were fixed at 20 °C and 4 M, respectively. For simplicity, both feed and draw streams were considered as calcium chloride aqueous solutions, whose activity was evaluated by the following exponential fitting ($R^2 \approx 0.99$) as function of molality $(m)^{28}$: $a_{CaCl_2} = -0.05893\, m^{1.32} + 1$. Then, without loss of generality, the Reynolds number was considered equal to 1000 (i.e., laminar regime), $\Omega = 0.01$, and the membrane characterized by $\delta_m = 77\,\mu m$, $\varepsilon = 0.83$ and $2r = 0.17\,\mu m$, which are common values for microporous hydrophobic membranes consistent with those tested experimentally in this work[29].

The impact of both molarity and temperature of the feed stream on the water vapor flux can be appreciated in Fig. 2a. In detail, an increase in the concentration and temperature of the feed stream leads to an increase in productivity, though to different extents. This observation is physically reasonable as

vapor pressure depends exponentially on temperature and roughly linearly on concentration, respectively. When the temperature of both streams is 20 °C, the full model (see Eq. (4)) reveals that a productivity of about 2.5 kg m^{-2} h^{-1} can be accomplished by employing a isotonic (i.e., $c_{b,f} \leq 100$ mM) feed stream and a concentrated (i.e., 4 M) draw stream. Under these circumstances, the comprehensive model developed in this study predicts the presence of a flux-induced temperature gradient across the membrane, which hinders the vapor flux. As a result, the draw solution becomes warmer than the feed solution, creating an opposing temperature gradient to the concentration gradient. This leads to an overall low driving force for water transport, impacting the efficiency of the process. Then, when $T_{b,f} = 70$ °C, a 120% higher productivity would be obtained with an isotonic feed stream compared with a 4 M one.
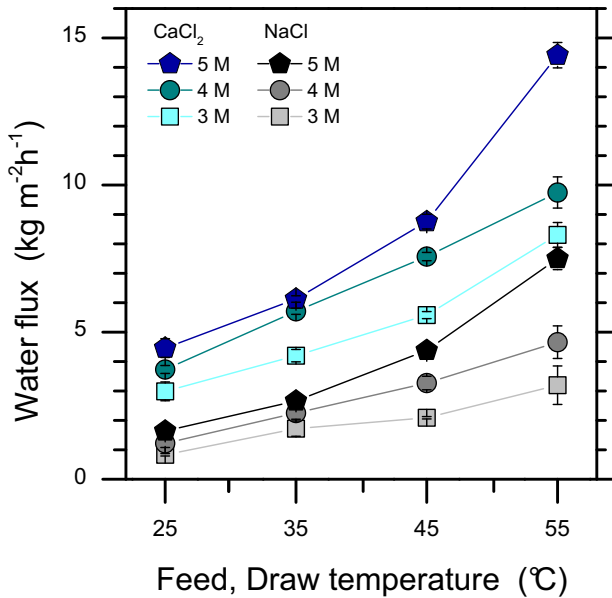
Fig. 3 Steady-state water vapor fluxes observed in osmotic distillation mode (OD, different salinity at equal feed and draw solution bulk temperatures) as a function of temperature and draw solute. Gray-scale symbols refer to NaCl as draw agent, while blue-scale symbols to CaCl$_2$. The investigated draw solute concentrations were 3, 4, 5 M for both agents. Lines connecting the data points are intended as a guide for the eye. All error bars represent ±1 s.d.

In Fig. 2b, the percent error between the results predicted by the full (Eq. (4)) and the linearized (Eq. (21)) model is reported. The percent error was evaluated as: $\Delta\% = \frac{J_{w,Eq.4} - J_{w,Eq.21}}{J_{w,Eq.4}}$. This comparative study is relevant to explore the benefits and limits of the simplified linear model. Indeed, the latter is widely preferred and employed by the scientific community since it requires only knowing two bulk quantities (i.e., molarity and temperature, more experimentally accessible than vapor pressure and activity) and, at most, reasonable values of the polarization coefficients (see Eq. (21)) from experimental fitting. Interestingly, the linearized model either overestimates or underestimates the productivity, depending on operating conditions. Specifically, the linear activity model (Eqs. (18) and (19)) increasingly overestimates activity values in the feed stream as molarity increases. This effect results in an overestimation of the driving force, hence an overestimation of productivity, as a function of feed molarity. From the draw stream perspective, on the other hand, employing the linear activity model always implies underestimating the driving force, for the same reasons. In the case study investigated here (i.e., 4 M CaCl$_2$ as draw stream), the underestimation of the activity amounts to 40%. As a result, for feed streams with molarity lower than about 1.5 M, the linear model underestimates the productivity obtained with the full model for any value of bulk feed temperature (i.e., positive $\Delta\%$ values in Fig. 2b). However, $\Delta\%$ values decrease as the bulk temperature gradient between the feed and draw streams increases. Indeed, the term introduced through the Clausius-Clapeyron equation (i.e., $\frac{dP}{dT}\big|_{\bar{T}_m}(T_{m,f} - T_{m,d})$) has a compensatory effect, as it overestimates the net value of the vapor pressure gradient to a gradually increasing extent as the bulk temperature gradient increases. For ΔT greater than or equal to about 35 °C (i.e., bulk temperature of the feed solution equal to about 55 °C, being $T_{b,d}$ equal to 20 °C) and feed molarity greater than about 1.5 M, the linear model always overestimates the values obtained with the full model, at least for the considered operating conditions. The two effects together result in overestimation of the

productivity (i.e., very negative $\Delta\%$ values in Fig. 2b) for high feed temperature and high feed molarity values.

It is worth noting that within a range of engineering-relevant values, specifically for feed molarity between 0 M and 2.5 M, and feed temperature between 40 °C and 70 °C, the discrepancy between the two models remains reasonably limited. In fact, the variation in $\Delta\%$ ranges from −20% (approaching the upper feed molarity values of the considered range) to +20% (approaching the lower feed molarity values). Note that, for lower feed temperatures and thus lower water vapor flux values, the absolute error between the two models is obviously limited— although $\Delta\%$ may be larger than ±20%. Therefore, at a practical level and for streamlined productivity assessments, the validity range of the linear model may also be extended for all conditions yielding low vapor flux values in addition to the ranges indicated above.

Experimental results and model validation

Experimental tests were conducted to robustly validate the proposed model and to gain a deeper understanding of the process. Specifically, the tests were performed in three modes: osmotic distillation (OD) with a driving force provided by concentration difference only; membrane distillation (MD) with a driving force provided by temperature difference only; osmotic membrane distillation (OMD) where the combined concentration and temperature differences provide the driving force. The experimental parameters were varied, including the bulk temperatures of the feed and distillate streams and the concentration of the draw solution on the distillate side. All the results discussed herein are steady-state values obtained at a constant flux[12].

Results of the OD tests are presented in Fig. 3. These results were obtained by solely utilizing the driving force exerted by the salinity difference, while maintaining an equal bulk temperature on both the feed and draw sides. Note that, despite the bulk temperature was the same at the two sides of membrane, its absolute value had a substantial impact on water flux, which increased monotonically in the range 25–55 °C. This effect has been also observed in previous studies, being mainly due to the decrease of mass transfer resistance (the higher the temperature, the higher the diffusion coefficient), and to the increase of water vapor pressure[30–32]. The measured increment in water flux is linear or superlinear with temperature, with the largest relative increase observed between 45 °C and 55 °C. Sodium chloride and calcium chloride were both investigated as draw agents[25]. As expected, the asymmetric solute—which formed three species in solution (Ca^{2+}, Cl$^-$, Cl$^-$)—leads to higher fluxes compared to NaCl, due to a higher osmotic pressure and thus lower activity of the draw solution, at the same solution molarity[33].

The 4 M CaCl$_2$ draw solution was then selected to perform additional tests in OMD and MD mode. As a matter of fact, hypersaline streams can ideally be used as draw solutions in OD and OMD applications, since no reverse solute flux should occur during the process[34]. Indeed, no or negligible reverse solute flux from the draw to the feed side was recorded in any of the experiments of this research, i.e., the electric conductivity of the feed solution did not change appreciably.

Results presented in Fig. 4a, b illustrate the same data but reported in two different ways to better unravel the phenomena that regulate the process. Figure 4a shows how the OMD water flux changed as a function of the temperature difference between the warm feed and the cold draw side. The color of symbols is associated with different draw solution temperatures, while empty symbols refer to a condition with no draw solute on the distillate side, i.e., pure MD mode. The arrows connecting the symbols were added to visualize the gain in productivity obtained in the OMD tests compared to each respective MD test. As expected, the water flux was larger if a larger temperature difference was maintained between the two membrane sides. However, contrary to the pure
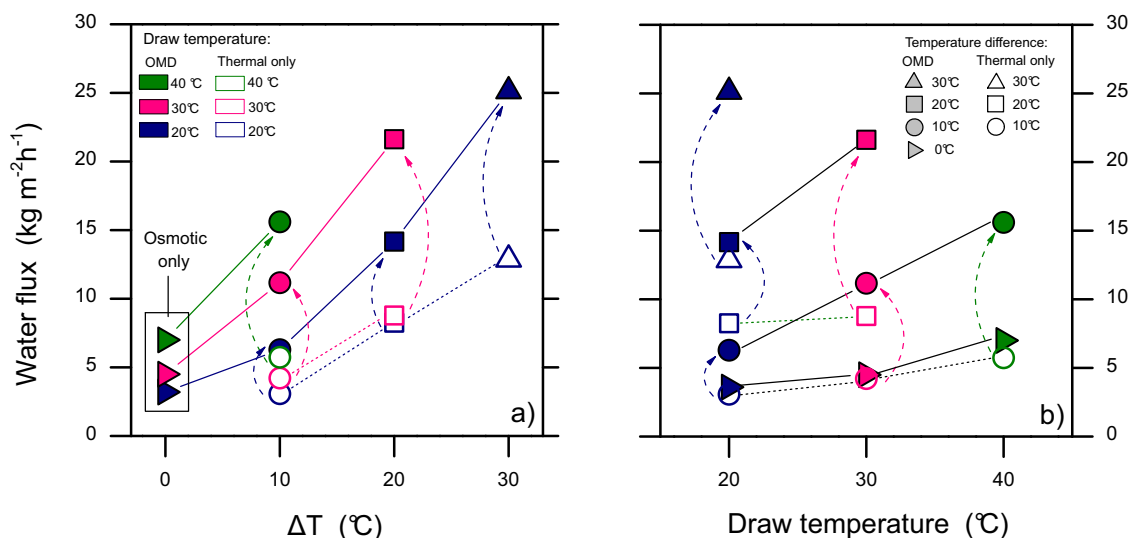
Fig. 4 Steady-state water vapor fluxes observed in osmotic membrane distillation (OMD, exploiting both thermal and salinity driving forces). a Water vapor flux values plotted as a function of the bulk temperature difference between the warm feed side and the cold draw side. **b** Water vapor flux values plotted as a function of the bulk draw solution temperature. In both graphs, green, pink, and blue symbols refer to bulk draw temperatures of 40 °C, 30 °C, 20 °C, respectively. Sideways triangles, circles, squares, and upright triangles refer to bulk temperature differences of 0 °C (pure OD), 10 °C, 20 °C, 30 °C, respectively. Solid symbols refer to the presence of a 4 M CaCl$_2$ in the draw side (OMD), while empty symbols to pure MD mode (same salinity on both sides). Dashed arrows connect each OMD data point with the respective MD data point, namely, data from test performed with analogous temperatures on either membrane side but with and without draw agent, respectively. The graphs actually report the exact same experimental data in two different visualizations to facilitate reading and to highlight different phenomena. All continuous lines connecting the data points are intended as guides for the eye.

MD case, this gain in productivity appeared to increase more than linearly for the OMD case as a function of bulk temperature difference. This effect can be also noticed in Fig. 4b, which shows how—for any fixed temperature of the draw solution (data sitting on the same column)—the distance between the pure MD and the OMD productivity is larger for vertical triangles with respect to squares and, in turn, to circles (bulk temperature difference of 30 °C, 20 °C, 10 °C, respectively). Also, for the same bulk temperature difference in Fig. 4a (data sitting on the same column), the increase in water flux is more pronounced for green with respect to pink and, in turn, to blue data points (bulk draw temperature of 40 °C, 30 °C, 20 °C, respectively).

The visualization in Fig. 4b allows for a comparison between the effects on productivity achieved by varying the temperature gradient alone and the productivity gained by including a draw solute. Let us analyze, for example, a pure MD mode with a bulk feed temperature of 40 °C and a bulk draw temperature of 20 °C, corresponding to a bulk difference of 20 °C and represented by the empty blue square. A higher increment in productivity can be achieved by using 4 M CaCl$_2$ in the draw side (solid blue square) than increasing the bulk feed temperature of 10 °C (empty blue triangle, corresponding to a bulk temperature difference of 30 °C). In another scenario, almost the same water flux can be achieved by operating in OMD mode with bulk feed and draw temperatures of 40 °C and 30 °C, respectively (represented by the solid pink circle, ~11.5 kg m^{-2} h^{-1}), compared to a pure MD situation with bulk temperatures of 50 °C and 20 °C (indicated by the empty blue triangle, ~13.5 kg m^{-2} h^{-1}). This observation suggests the possibility of reducing the energy required to heat the feed and/or cool the distillate solution by harnessing the salinity gradient between the streams in the OMD process.

In Fig. 5, the experimental results (marked with symbols) just discussed are finally compared to the prediction of the Maxwell-Stefan and dusty-gas theoretical model (Eq. (4)), graphically represented through shaded areas. Steady-state specific water vapor flow rates were considered for two operating modes as a function of the bulk temperature of the feed stream, under different bulk temperature values of the draw stream. In detail,

Fig. 5a shows productivities when pure water flows in both channels with the temperature being the only driving force (i.e., MD mode); whilst Fig. 5b shows the productivity of the OMD process, where pure water and 4 M CaCl$_2$ aqueous solution flow in the feed and draw channels, respectively. Overall, Fig. 5a, b prove the good agreement between the experimental and modeling data for both the MD and the OMD modes.

The upper limit of the shaded areas was obtained by setting the polarization coefficients (i.e., θ_T, $\theta_{s,f}$, $\theta_{s,d}$) equal to 1. This delineates the maximum productivity that can be thermodynamically achieved by these processes in the ideal situation where no transport-limiting phenomena occur. Indeed, the ideal upper boundary represents the theoretical maximum productivity achievable by the process, which serves as a reference point for optimizations. While improvements can be made to enhance the efficiency of the process, the ideal upper boundary serves as a limit that cannot be surpassed. On the other hand, the lower limit describes the productivity achieved by setting all the polarization coefficients equal to 0.4. This value was reasonably chosen as the minimum threshold to be guaranteed during the module design stage. This lower limit provides a practical reference for the expected productivity while accounting for certain transport-limiting phenomena. Note that, in the scenario described in Fig. 5a, only temperature polarization (i.e., θ_T) would eventually be observed. Furthermore, the experimental results were fitted to the theoretical model using a non-linear least-squares solver, with the polarization coefficients as the fitting parameters (θ_T^{FIT} and $\theta_{s,d}^{FIT}$). The fitting curves are depicted as solid lines in Fig. 5. In the MD mode (Fig. 5a) with T_{draw} at 20 °C and 30 °C, the fitting parameter θ_T^{FIT} had values of 0.56 and 0.44, respectively. In the OMD process (Fig. 5b), with T_{draw} at 20 °C, θ_T^{FIT} and $\theta_{s,d}^{FIT}$ were 0.90 and 0.94, respectively. For T_{draw} at 30 °C, θ_T^{FIT} and $\theta_{s,d}^{FIT}$ were 0.80 and 0.99, respectively. These fitted parameters allow for a closer alignment between the experimental data and the theoretical model, providing valuable insights into the process behavior.
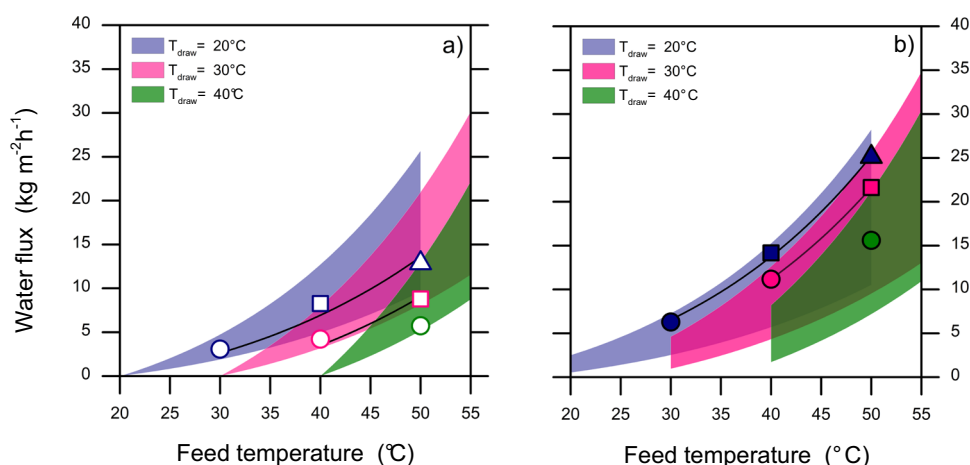
Fig. 5 Comparison between experimental (symbols) and model (shaded areas) results. Two scenarios were considered, that is, (**a**) a case where pure water flows in both channels with the temperature being the only driving force (i.e., MD mode), and (**b**) the OMD case, where pure water and 4 M $CaCl_2$ aqueous solution flow in the feed and draw channels, respectively. Steady-state specific vapor mass flow rates J_w were reported as function of the bulk temperature of the feed stream, under different bulk temperature values of the draw stream (i.e., T_{draw}). The shaded area represents the prediction of the model between the thermodynamic upper limit and the case with polarization coefficients equal to 0.4. The lines are the best fit of the experimental data using the polarization coefficients as fitting parameters. The same color and symbol code was used in presenting the results here and in Fig. 4.
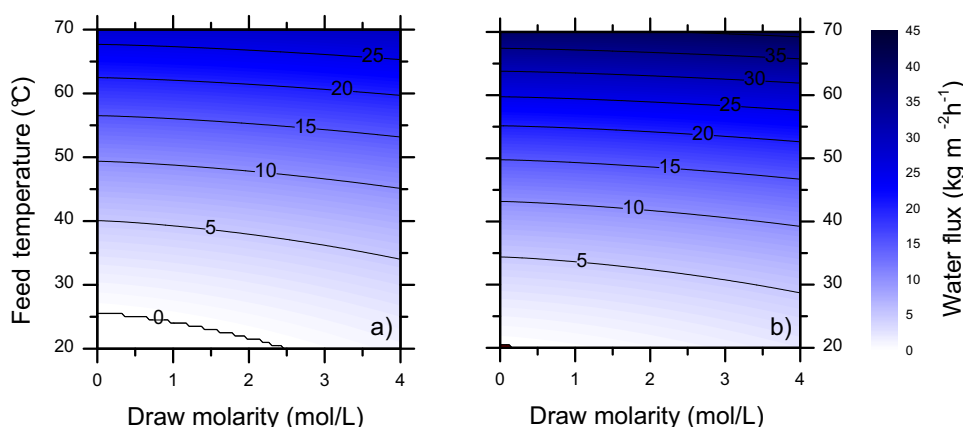

Fig. 6 Potential applications of the OMD process. Sensitivity analyses on productivity considering (**a**) 4 M LiCl-based and (**b**) 154 mM NaCl-based aqueous solutions as feed stream, and $CaCl_2$-based aqueous solution as draw stream. The draw solution temperature was set equal to 20 °C. The results were obtained by applying Eq. (4). The membrane characteristics used for the calculations were those of the PTFE membrane deployed in the experiments.

Productivity and effect of different driving forces

The OMD process holds promising applications in various fields. For instance, it can be employed for dewatering wastewater or brine to concentrate and then extract valuable metals effectively, or the process can be utilized for the concentration of organic substances in biological or beverage solutions[34]. In Fig. 6a, the specific water vapor mass flow rates achieved by considering 4 M LiCl-based and $CaCl_2$-based aqueous solutions as feed and draw, respectively, were calculated by Eq. (4) under a varying range of both draw molarity and feed temperature. For the lithium chloride aqueous solutions, activity values were determined as a function of molality by the following fitting equation ($R^2 \approx 0.99$)[28]: $a_{LiCl} = -0.0035\,m^2 - 0.0331\,m + 1$. The results indicate that, as the draw molarity values decrease, the bulk temperature of the feed stream should be increased to maintain constant productivity. The limiting case, which is characterized by zero flux withdrawn from the feed stream, occurs for draw molarity values approximately equal to 2.46 M, assuming the bulk feed temperature equal to 20 °C. Then, for draw molarity values approaching zero, the

minimum bulk feed temperature needed to avoid negative flux (i.e., water transport from the draw to the feed side) is about 25 °C. The maximum productivity value achieved within the investigated range was ~29.7 kg m^{-2} h^{-1}. This value was computed for a feed temperature of 70 °C and a draw molarity of 4 M.

Furthermore, it is important to emphasize that utilizing a high draw solution molarity offers the advantage of potentially reducing the bulk temperature of the feed stream while maintaining productivity. This approach results in increased energy savings, as less energy is required to heat the feed stream to achieve the desired water vapor flux through the membrane. Specifically, for a bulk temperature of the feed stream equal to 30 °C and draw molarity approaching zero, the achievable productivity amounts to about 1.27 kg m^{-2} h^{-1}. The same value might instead be attained by exploiting the driving force exerted by a 4 M draw solution and thus lowering the bulk temperature of the feed stream to 20.5 °C, which would be equivalent to a 95% energy saving, assuming the same feed flow rate, specific heat capacity, and considering 20 °C as initial feed solution temperature. On the other hand, results highlight how the marginal utility

of working with higher draw molarities diminishes when bulk feed temperature values also increase. In other words, the benefits gained from increasing the draw molarity become less important when the feed stream is already at higher temperatures. For instance, a productivity of 27.4 kg m^{-2} h^{-1} might be attained either through operating with a bulk feed temperature of 70 °C and about zero draw molarity or through operating with a 4 M draw solution and only slightly lowering the bulk feed temperature, reducing only by 5% the energy required by the OMD process.

For completeness and to explore the productivity of another interesting exemplifying application of OMD, the specific water vapor mass flow rates calculated considering a realistic isotonic solution as feed stream are reported in Fig. 6b. Here, without loss of generality, a 154 mM NaCl aqueous solution was considered. The activity values as function of the molality were evaluated by the following fitting equation ($R^2 \approx 0.99$)[28]: $a_{NaCl} = -0.0017\,m^2 - 0.0304\,m + 1$. In this scenario, negative specific water vapor mass flow rates (i.e., dilution of the feed stream) were observed only for 120 mM draw solutions and bulk feed temperature equal to 20 °C. The qualitative productivity trend is quite comparable to that described in Fig. 6a, while higher productivity values were observed. For bulk feed temperature equal to 70 °C and 4 M draw solutions, 41.2 kg m^{-2} h^{-1} was achieved, namely, 38% more than the best result in Fig. 6a.

Limitations and efficiency of the process

Finally, the effect of the polarization phenomena was explored in Fig. 7 to gain additional insight into the potential, efficiency, and thermodynamic limitations of the OMD process. The calculations were performed for the same two scenarios described in Fig. 6. In particular, the percentage water flux loss due to polarization, defined as $\zeta_\% = \frac{J_{w,ideal} - J_w}{J_{w,ideal}}$, was calculated using 4 M LiCl-based (Fig. 7a) or 154 mM NaCl-based (Fig. 7c) aqueous solutions as feed streams. $J_{w,ideal}$ refers to the productivity computed by imposing polarization coefficients equal to 1 (thermodynamic limit of the water transport), whilst J_w refers to the actual productivity calculated by the OMD model.

As feed temperature and/or draw molarity increase, the absolute difference between $J_{w,ideal}$ and J_w increases (see Supplementary Note 1), although with a different magnitude. This result is expected since polarization increases with flux, resulting in larger relative losses when the absolute values of the observed flux increase. From an engineering standpoint, this well-known phenomenon results in the need of operating within a reasonable range of driving force (i.e., not overly high), to avoid using impractically high amounts of "external" (e.g., heat) or "internal" (e.g., draw concentration) energy to obtain higher fluxes, which could lead to increased costs and operational challenges.

Considering the parameter $\zeta_\%$, instead, the trend of relative losses helps understanding the OMD process from a thermodynamic standpoint and deserves here to be deepened through a comprehensive discussion. In Fig. 7a, $\zeta_\%$ is reported when considering a 4 M LiCl aqueous solution as feed stream, which is a relevant case study for the concentration of metals in brine or high-salinity waste liquid streams. At low bulk feed temperature values, J_w ranges from negative (not reported in Fig. 7a, see white area) to positive values, as the draw molarity increases. At the transition line, J_w is nearly zero, while $J_{w,ideal}$ is only slightly higher, which leads to $\zeta_\%$ values equal to roughly 100%. Moving toward higher draw molarity values (from left to right in the color map), the percentage increase of $J_{w,ideal} - J_w$ is lower compared to the percentage increase of $J_{w,ideal}$, thus $\zeta_\%$ decreases, suggesting that the process becomes intrinsically more efficient in terms of productivity from a thermodynamic standpoint. On the other hand, at higher bulk feed temperature values (moving from bottom to top in the color map), the impact of concentration-

related driving force on the productivity becomes negligible compared to that of the driving force induced by the temperature difference across the membrane. Consequently, the variation of $\zeta_\%$ is less significant as draw molarity changes. That is not to say that concentration polarization effects are negligible at high feed temperature, but that flux values are governed mostly by temperature-induced driving force; see next paragraph.

In Fig. 7b, the partial linearized contribution of temperature (i.e., θ_s equal to 1) and concentration (i.e., θ_T equal to 1) polarization phenomena to the full polarization loss is reported through the parameter R, which is defined as $R = \frac{(J_{\theta_T=1} - J_w) - (J_{\theta_s=1} - J_w)}{(J_{w,ideal} - J_w)}$. R ranges from -1, when $J_{\theta_s=1}$ and $J_{\theta_T=1}$ tend to $J_{w,ideal}$ and J_w, respectively, to 1, when $J_{\theta_T=1}$ and $J_{\theta_s=1}$ tend to $J_{w,ideal}$ and J_w, respectively. As a result, the parameter R encompasses a range of conditions, from cases where losses due to concentration polarization dominate to situations where temperature polarization effects are primarily responsible for flux reduction. The variation of R reflects the interplay between these two phenomena and their relative impact on the effective water vapor flux in the OMD process.

Overall, within the investigated range of feed temperature and draw molarity values, losses due to temperature polarization phenomena are found to be dominant compared to those related to the concentration-based driving force, i.e., the shade of the color map is mostly blue and values of R are always positive. However, when the driving force is increased, regardless of its nature, the relative contribution of concentration polarization becomes gradually more important and R decreases in value approaching zero for high draw molarity both at low and at high feed temperature values, i.e., the color map becomes gradually lighter as we move from left to right and from bottom to top. Interestingly, there is a region, corresponding to bulk feed temperatures between roughly 25 °C and 45 °C, for which the magnitude of temperature polarization is always highly dominant compared to that of concentration polarization, even at high draw molarity. Also interestingly, the temperature-dependent polarization coefficient is high under conditions whereby the driving force is only exerted by the molarity difference (i.e., for $T_{b,f} = T_{b,d} = 20$ °C), and draw molarity values are around 2.46, i.e., the threshold which generates positive flux when the feed and draw bulk temperature solutions are equal. Indeed, despite the absence of a bulk temperature difference between the two sides of the membrane, for low bulk feed temperature and high draw molarity values, an evaporative cooling phenomenon[35] is established due to the phase change of water, therefore leading to an increase in the draw temperature and a decrease in the feed temperature caused by water flux (see Supplementary Note 1).

The results presented in Fig. 7a, b, combined with the expected flux values, suggest that there may be a region of higher efficiency for medium values of the bulk feed temperatures and high draw molarity values when dewatering feed solutions of high concentration. In that region, flux losses due to polarization are relatively low and the use of a draw agent is justified by increased productivity not accompanied by a substantial relative contribution of the concentration polarization effect to flux loss. On the other hand, using a draw agent may not be worthwhile when the driving force is already high due to large values of the bulk feed temperature. Indeed, these observations precisely support the synergistic combination of temperature and concentration-related driving forces with the goal to minimize the temperature gradient, hence the use of thermal energy, in the OMD process. Ultimately, operating conditions should be chosen based also on engineering and practical considerations, but the thermodynamic aspects discussed above may be highly relevant to design an efficient system.

In Fig. 7c, $\zeta_\%$ is reported considering a 154 mM NaCl aqueous solutions as feed stream, that is a case study relevant for solutions
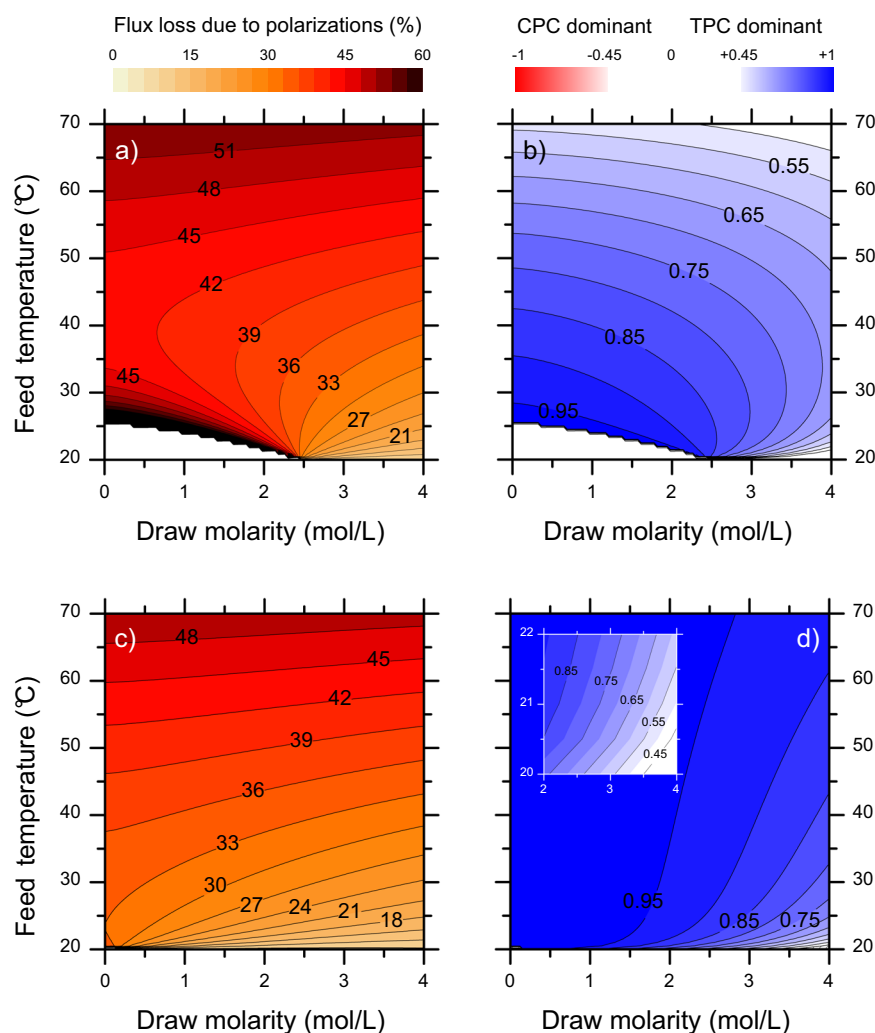
Fig. 7 Effect of polarization phenomena on productivity. Considered feed stream: **a**, **b** 4 M LiCl-based aqueous solution; **c**, **d** 154 mM NaCl-based aqueous solution. In detail, panels (**a**) and (**c**) quantify the relative water vapor flux loss due to polarization defined as $\frac{J_{w,ideal} - J_w}{J_{w,ideal}}$, where $J_{w,ideal}$ was obtained imposing θ_T and θ_s equal to 1. Panels (**b**) and (**d**) quantify, through the parameter $-1 \leq R \leq 1$, the partial linearized contribution of temperature (i.e., θ_s equal to 1) and concentration (i.e., θ_T equal to 1) polarization phenomena to the full polarization loss. This parameter is defined as $R = \frac{(J_{\theta_T=1} - J_w) - (J_{\theta_s=1} - J_w)}{(J_{w,ideal} - J_w)}$. The results were obtained by considering a CaCl$_2$ aqueous solution as draw at bulk temperature of 20 °C. The membrane characteristics used for the calculations were those of the PTFE membrane deployed in the experiments. See Supplementary Note 1 for detailed trends of the polarization coefficients, the temperature difference across the hydrophobic membrane (ΔT_m), and the ideal ($J_{w,ideal}$) and effective (J_w) yields, in the two considered case studies.

at or close to isotonicity, e.g., human plasma, beverages, and other biological solutions. Compared to the former case, negative water flux values are limited to draw molarity below 120 mM and a bulk feed temperature of 20 °C. Also, flux loss due to polarization effects are generally smaller compared to the case discussed in Fig. 7a, given the lower magnitude of concentration polarization on the feed side. That being said, the trends are comparable to those of the former case, with relative losses increasing predominantly at larger values of bulk feed temperatures (moving from bottom to top) being the driving force dominated by the temperature gradient in the uppermost part of the graph. While trends of relative total losses due to polarization are not too dissimilar in the case of a concentrated (Fig. 7a) and a more diluted (Fig. 7c) feed stream, the relative contribution of temperature and concentration polarization is strikingly different in the two cases. In Fig. 7d, the corresponding R is reported for the case of 154 mM NaCl aqueous solutions as feed stream. Also in this case, temperature polarization effects are dominant all across the color map, but this dominance is even more pronounced: due

to the reduced concentration polarization phenomena in the feed channel, R assumes higher values (it is closer to 1) with respect to the previous case. The contribution of concentration polarization becomes large only for low values of bulk feed temperature and high values of draw molarity at the same time, with R gradually decreasing and becoming equal to 0.32 at the bottom right corner of the graph.

Therefore, in the case of a feed stream with low concentration, the optimization of thermodynamic efficiency is less obvious compared to the former case. The results presented in Fig. 7c, d, combined with the expected flux values, suggest that the region of higher efficiency may correspond to low-medium bulk feed temperatures and medium-high draw agent concentrations. However, in this range, expected fluxes would be relatively low. As a result, engineering and practical considerations, e.g., related to the required total system productivity or the nature of the feed mixture, would likely control the operating conditions.

To assess the potential and the challenges of OMD, long-term membrane behavior and process optimization should be carefully

investigated in each specific, possible application. Although fouling, scaling, and wetting phenomena have not yet been adequately investigated, well-known mechanisms in direct contact membrane distillation may be considered relevant in OMD as well. Therefore, hydrophobic substances are more likely to interact with the hydrophobic membranes, potentially causing fouling. In addition, the presence of surfactants and any other phenomena that would induce pore wetting in membrane distillation would also impair the separation capabilities of the OMD membrane, including the formation of crystals within its pores. Additional issues may arise in OMD due to scaling and crystallization of the draw agent on the distillate side of the membrane, which differs from typical membrane distillation processes. The use of an antiscalant may thus be required, especially in cases when the draw solution is highly concentrated. On the other hand, working at lower temperature on the evaporator side would reduce the probability of scaling of the feed stream compared with a typical membrane distillation operation, and this potential advantage may be critical for complex solutions for which scaling control is problematic. With respect to process optimization, the presence of the draw agent in OMD may provide more flexibility in the management of the thermal energy on the feed side, while simultaneously creating issues of draw solution selection, management, and possible reconcentration. These issues should be studied in more detail with the support of sustained research efforts around OMD.

In this study, we investigate the potential, efficiency, and thermodynamic limitations of the OMD process by means of extensive theoretical and experimental analyses. OMD is an extension or variant of the more conventional and well-known MD process, where a temperature gradient is imposed between two solutions to generate a water vapor flow from a concentrated solution to a freshwater solution. In contrast, in the OMD process, concentration and temperature gradients are synergically exploited to generate a water vapor flow from a feed dilute stream to a draw concentrated stream, through a hydrophobic membrane. Therefore, OMD is particularly suitable for applications that do not require draw solution regeneration, such as in the separation, concentration, and dewatering of liquid streams to concentrate valuable elements and compounds. Despite the potentially beneficial impact of this process in pursuing zero liquid discharge, resource recovery, and sustainable socio-economic growth, the available literature has theoretical gaps regarding OMD, particularly concerning the intertwined heat and mass transfer processes.

In response to this gap, here we have developed two new OMD models, each offering a distinct level of detail, flexibility, and applicability range. These models have been designed to cater to different research needs and practical applications, providing researchers and engineers with a range of options to explore and analyze the OMD process comprehensively. In detail, we propose for the first time, to the best of our knowledge, a comprehensive model of the OMD process, directly derived from the Maxwell-Stefan and Dusty-gas equations, which does not include simplifications. Subsequently, a simplified, linear model based on the Clausius-Clapeyron equation is developed discussing its strengths and limits. The latter, although requiring knowledge only of bulk quantities (i.e., molarity and temperature) and polarization coefficients, exhibits varying discrepancies from the predictions of the full model as concentration and temperature vary. Discrepancies were thus discussed to identify the ranges of applicability of the simplified model. In addition, experimental water vapor fluxes were measured under varying operating conditions, with the purpose of validating the model. The model adequately predicted the experimental fluxes and identified the highest possible fluxes at the thermodynamic limits. The theoretical and experimental analyses were further used to explore and reveal the influence of process parameters, such as bulk temperature and molarity of the two streams, on the transmembrane water vapor flux. Finally, we examined the effects of concentration and temperature polarization on driving force reduction (flux loss) under various operating conditions. The complex nature of conjugate heat and mass transfer leads to non-trivial trends, necessitating detailed investigations for a comprehensive understanding and optimization of the OMD process. In detail, the model interestingly predicts temperature polarization coefficients higher than one or negative under some operating modes, the latter being induced by evaporative cooling phenomena. Note that the membrane deployed in this study, whose characteristics were also used as model parameters to perform sensitivity analyses and OMD flux evaluations, was designed for traditional membrane distillation and may not be ideal for an OMD process. Indeed, improvements in membrane properties, specifically tailored for OMD, may increase the efficiency and reduce some of the limitations of this innovative process, compared to what exemplified in this work.

The major strengths and prospected applications of OMD based on our findings are as follows:

1. Ability to produce higher water vapor fluxes compared to conventional processes like osmotic dilution and forward osmosis. For instance, considering pure water and 4 M $CaCl_2$ aqueous solution flowing in the feed and draw channels, respectively, with a draw temperature of 20 °C, OMD can ideally produce about 3.7 kg m^{-2} h^{-1}, while osmotic dilution mode yields only 2.5 kg m^{-2} h^{-1}. This represents a 50% productivity increase in OMD with a minor 3 °C increase in feed temperature while keeping other conditions fixed.
2. Ability to utilize lower feed temperatures, resulting in significant energy savings, ranging from 5 to 95%, depending on the operating conditions. This feature is especially relevant when managing temperature-sensitive high-value compounds, as found in the food and beverage, nutraceutical, and cosmetics industries.
3. Ability to employ draw solutions with extraordinarily high concentrations. As flux occurs via a vapor pressure gradient across a hydrophobic membrane, OMD is not susceptible to reverse solute diffusion to the feed stream, unlike forward osmosis, where osmotic pressure drives flow across a hydrophilic membrane. Management of the diluted draw solution may be a complex issue in some instances, and this topic is not investigated here. However, OMD may be an advantageous process especially when draw solution regeneration is not needed (e.g., use of a sacrificial draw solution, achievement of minimal dilution) or when it can be accomplished by simple means (e.g., replenishment of inexpensive draw agent into solution).

Overall, these strengths highlight the potential of OMD in entering the portfolio of liquid separation processes that are likely to offer enhanced efficiency, reduced energy consumption, and improved resource recovery toward the sustainable target of zero liquid discharge water treatments.

That being said, outstanding challenges for OMD implementation exist, for example, (i) the need for a comprehensive and effective investigation of fouling, scaling, and wetting mechanisms with specific, relevant feed streams, (ii) the intrinsically low rejection of volatile compounds that would translate into draw solution contamination and potential cross-contamination of the feed streams, (iii) selection, management, and possible reconcentration of the draw solution, (iv) the need for process optimization via combined modeling and experimental testing, ideally at pilot scale, (v) the necessity for currently lacking techno-economic evaluations based on wide-ranging and robust data, which should suggest feasible implementations of OMD as well as those that are likely to be unsuccessful from an economic standpoint. OMD costs may be envisioned as not too dissimilar to those of membrane distillation installations, with additional expenses around draw solution utilization and simultaneous savings in terms of thermal

energy needs, which should be evaluated on a case-by-case basis. While some of the issues highlighted above, as well their potential solutions, are common among all thermally driven membrane-based separation processes or among all osmotically driven ones, others are unique to OMD and necessitate targeted investigation.

METHODS

Naming convention

The transport behavior in the OMD process is discussed in this work through a combination of modeling and experimental analyses. Since literature studies use different naming conventions, a brief explanation of the process is reported here together with the adopted terminology. In OMD, two solutions are in contact with a hydrophobic membrane. The warmer *feed* solution is separated from the colder *draw* solution of higher salinity by the membrane. In this study, the investigated feed solution is aqueous. Specifically, pure water was used in the experiments while different aqueous mixtures were assessed by means of the developed model. Therefore, in the relevant instance of this study, the draw solution is enriched by the condensation of water vapor during the OMD process. Pure water vapor passes through the membrane due to the vapor pressure gradient created by temperature and salinity differences between the two sides of the membrane.

Bench-scale OMD setup

The OMD process was investigated experimentally utilizing a bench-scale membrane distillation cell of the following dimensions: length 75 mm, width 28 mm, and height of the flow channels 2 mm. The module hosted a rectangular hydrophobic polytetrafluoroethylene (PTFE) membrane with a thickness of 77 μm, nominal pore size of 0.17 μm, and a total active area of 21 cm². The membrane used in the experiments was manufactured for membrane distillation processes and did not necessarily have the best characteristics to maximize the output in an osmotic membrane distillation process. Ideal OMD membranes may likely be characterized by smaller thickness and different porosity compared to materials designed for traditional membrane distillation. The experimental setup was also composed by two heat exchangers, which allowed heating up and cooling down to the target temperatures the feed and the draw solution, respectively. The system worked under atmospheric pressure with negligible pressure losses due to friction. The feed and draw solution tanks were sealed with lids to prevent water vapor from escaping, while also ensuring a continuous air inlet to avoid pressurization. A constant cross-flow rate was maintained during the tests utilizing two volumetric pumps controlled by inverters. The water vapor flux through the membrane was determined by measuring the time-dependent weight change of the draw tank using a computer-interfaced balance. The initial feed and draw solution volumes were both equal to 1 L.

Experimental protocol

The filtration experiments were performed at a circulation flow rate of the feed and draw solutions equal to 20 L h^{-1}, which corresponded to a cross-flow velocity of roughly 0.065 m s^{-1}. The reported water flux data are taken as the average value obtained with individual measurements performed every 10 min for 1 h, at steady-state. Firstly, six osmotic distillation experiments were performed, whereby only the difference in salinity between the feed and draw solution was exploited as driving force, i.e., the two solutions had the same temperature. Specifically, temperatures were kept equal to 25 °C, 35 °C, 45 °C, or 55 °C, while the tested draw agents were 3 mol L^{-1}, 4 mol L^{-1}, and 5 mol L^{-1} sodium chloride or calcium chloride. High purity sodium chloride and calcium chloride salts were purchased from Carlo Erba, Italy, and used to prepare the

draw solutions. Secondly, six membrane distillation experiments were performed, whereby only the temperature difference across the membrane was exploited as driving force. Temperature differences in the bulk of the solutions equal to 10 °C, 20 °C, and 30 °C were assessed, achieving a feed water temperature up to 50 °C. Lastly, three OMD experiments were performed with the same temperature ranges exploited for the second set of tests and using as draw agents those that provided the highest water fluxes according to the first set of experiments. Prior to each test, pure water was employed as the draw agent, and the same temperature was applied to both sides of the membrane to ensure that no water flux was observed in the absence of temperature or osmotic-driven forces. This step also facilitated the establishment of hydrodynamic equilibrium within the testing membrane cell[36]. This protocol was conducted again at the end of each experiment to ensure that irreversible membrane wetting did not occur during the test. Furthermore, since pure water was always utilized as feed solution, feed side electrical conductivity was monitored over time using an immersed probe (COND 7+, XS Instruments, Italy) to verify the absence (or negligible occurrence) of reverse salt flux from the draw to the feed solution.

Mass transport through the membrane

The Maxwell-Stefan and dusty-gas models were combined to evaluate the specific vapor mass flow rate through the membrane (J_w [kg m^{-2}h^{-1}])[37–41]. The Maxwell-Stefan model accounts for the external driving force, including the concentration effect (i.e., the chemical potential) and the molecular diffusion, which details the interaction between gas molecules. The dusty-gas model considers the interaction between gas molecules and the porous membrane (i.e., the collision between gas molecules and membrane pore walls). As a result of the combination of the aforementioned models, species transport through the porous membrane can be modeled as:

$$-\frac{x_i}{RT}\frac{d\mu_i}{dz} = \sum_{j=1, j\neq i}^{n}\left(\frac{x_j N_i - x_i N_j}{\frac{P\epsilon_m D_{ij}}{RT\tau}}\right) + \frac{N_i}{\frac{P\epsilon_m D_{i,K}}{RT\tau}} \tag{1}$$

where x_i and μ_i are the mole fraction and chemical potential of species i, respectively. Moreover, R is the molar gas constant; T and P are the absolute temperature and the total pressure of the mixture; z is the vertical coordinate (Fig. 1). At the second member of the equation, the two terms represent the contributions of molecular diffusion and Knudsen diffusion, respectively. In detail, D_{ij} is the diffusion coefficient of species i in species j and $D_{i,K}$ is the Knudsen diffusion coefficient for species i. The latter can be written as $D_{i,K} = \frac{8r}{3}\sqrt{\frac{RT}{2\pi M_i}}$, being r the average pore radius of the porous membrane and M_i the molar mass of species i. Furthermore, N_i is the molar flux of species i. The parameters ϵ_m and τ are characteristic of the membrane and represent its porosity and tortuosity. The two parameters may be empirically correlated by considering the Mackie-Meares equation[42,43], namely, $\tau = \frac{(2-\epsilon_m)^2}{\epsilon_m}$. It is worth noting that the viscous contribution to vapor transport was not considered in this model because of the absence of a total pressure gradient across the porous membrane. Furthermore, hydrophobicity prevents pore penetration and thus the establishment of viscous flow.

As proposed in the literature[37–41,44], Eq. (1) can be simplified by relying on reasonable assumptions. In detail, it may be assumed that: (i) the ternary mixture of water vapor, nitrogen, and oxygen is an ideal binary mixture of water vapor and air; and (ii) the air molecules occupying the membrane pores are static, as a consequence of the low solubility of air in water. Then, the chemical potential of water vapor, being considered ideal, may be expressed as $\mu_w = \mu_{w,pure} + RT \ln x_w$, where the subscript w refers to water vapor. Following these assumptions, Eq. (1), circumscribed to the process

under consideration, is re-written as follows:

$$-\frac{dx_w}{dz} = \frac{(1-x_w)N_w}{\frac{P\epsilon_m D_{w,a}}{RT\tau}} + \frac{N_w}{\frac{P\epsilon_m D_{w,K}}{RT\tau}} \qquad (2)$$

where $D_{w,a}$ and $D_{w,K}$ are the molecular diffusion of water vapor in air and the Knudsen diffusion of water vapor through the pores of the membrane, respectively. Considering the subscripts f, d, and m denoting feed, draw, and membrane, respectively, Eq. (2) can be integrated across the membrane:

$$-\int_{z_{m,f}}^{z_{m,d}} \frac{dx_w}{1-x_w+a} = \int_{z_{m,f}}^{z_{m,d}} \frac{N_w dz}{\frac{P\epsilon_m D_{w,a}}{RT\tau}} \qquad (3)$$

whereby $a = \frac{D_{w,a}}{D_{w,K}}$. In Eq. (3), $x_{w,m,f} = \frac{a(x_{s,m,f})p_v(T_{m,f})}{P}$ at $z = z_{m,f}$ and $x_{w,m,d} = \frac{a(x_{s,m,d})p_v(T_{m,d})}{P}$ at $z = z_{m,d}$ were the chosen boundary conditions, being a and p_v the activity and the partial water vapor pressure of the solution under consideration, respectively. The activity strongly depends on the mole fraction of the solute in the aqueous solution x_s, whilst the p_v depends on the temperature of solutions. Therefore, the non-volatile solute mole fractions and the temperature at the interfaces between the feed/draw aqueous solutions and the membrane (i.e., $x_{s,m,f}, x_{s,m,d}$ and $T_{m,f}, T_{m,d}$, respectively) were appropriately estimated to assess the net driving force of the process. Indeed, the values in the proximity of the membrane are different from the corresponding bulk values (hereafter denoted with subscript b) because of the formation of boundary layers.

The resulting analytical formulation governing the molar flux of water vapor through the membrane was subsequently derived after solving Eq. (3):

$$J_w = \psi \ln\left(\frac{1+a-x_{w,m,d}}{1+a-x_{w,m,f}}\right) \qquad (4)$$

where $J_w = N_w M_{H_2O}$, being M_{H_2O} the molar mass of water, $\psi = \frac{M_{H_2O}P\epsilon_m D_{w,a}}{RT\tau\delta_m}$, and δ_m the thickness of the membrane. ψ is the integration constant which encompasses all membrane characteristics as well as the absolute temperature and total pressure of the mixture.

Heat transfer through membrane and boundary layers

The total heat flux through the membrane is due to both the latent heat transfer related to the water vapor flux J_w and the heat conduction through the porous membrane. The thermal conductivity of the membrane can be estimated by a weighted mean, namely $k_m = k_{air}\epsilon_m + k(1-\epsilon_m)$, being k_{air} and k the thermal conductivity of the air trapped in the pores and of the material of the membrane, respectively. Thus, the steady-state heat transfer across the whole module, including the feed and draw channels, can be summarized as:

$$h_f(T_{b,f} - T_{m,f}) = \frac{k_m}{\delta_m}(T_{m,f} - T_{m,d}) + J_w \Delta H(\tilde{T}_m) = h_d(T_{m,d} - T_{b,d}) \qquad (5)$$

where h_f and h_d are the convective heat transfer coefficients in the boundary layers of the feed and draw channels, and $\Delta H(\tilde{T}_m)$ the latent heat of vaporization evaluated considering the average temperature in the membrane (i.e., $\tilde{T}_m$). By manipulating Eq. (5), the temperature at the feed/membrane and membrane/draw interfaces are derived:

$$T_{m,f} = \frac{\frac{k_m}{\delta_m}\left(T_{b,d} + \frac{h_f}{h_d}T_{b,f}\right) + h_f T_{b,f} - J_w \Delta H(\tilde{T}_m)}{\frac{k_m}{\delta_m} + h_f\left(1 + \frac{k_m}{\delta_m h_d}\right)} \qquad (6)$$

$$T_{m,d} = \frac{\frac{k_m}{\delta_m}\left(T_{b,f} + \frac{h_d}{h_f}T_{b,d}\right) + h_d T_{b,d} + J_w \Delta H(\tilde{T}_m)}{\frac{k_m}{\delta_m} + h_d\left(1 + \frac{k_m}{\delta_m h_f}\right)} \qquad (7)$$

The resulting temperature polarization coefficient can be thus evaluated as $\theta_T = \frac{T_{m,f} - T_{m,d}}{T_{b,f} - T_{b,d}} = \frac{\Delta T_m}{\Delta T}$. In case of $h_f = h_p = h$, the latter expression is simplified as $\theta_T = \frac{h - \frac{2J_w\Delta H}{\Delta T}}{2\frac{k_m}{\delta_m} + h}$, thus $T_{m,f} = T_{b,f} - \frac{\Delta T}{2}(1-\theta_T)$ and $T_{m,d} = T_{b,d} + \frac{\Delta T}{2}(1-\theta_T)$. The latter temperatures can be used to evaluate the effective vapor pressure at the membrane interfaces through the Antoine equation:

$$\log_{10}\left[p_v(T_{m,f/d})\right] = A - \frac{B}{C + T_{m,f/d}[^\circ C]} \qquad (8)$$

Relationships between the temperature in the bulk and at the feed/draw aqueous solutions-membrane interfaces can be obtained using heat transfer empirical correlations, such as $Nu = \frac{hd_h}{k} = f\left(Re, Pr, \frac{d_h}{L}\right)$, where Nu, Re, and Pr are Nusselt, Reynolds and Prandtl numbers, respectively, while d_h and L are the hydraulic diameter and the length of the module. To generalize the problem, the aspect ratio parameter $\Omega = \frac{d_h}{L}$ was introduced to account for the geometry of the module. The following correlations suggested by the literature were used for laminar and turbulent flow[45]:

$$Nu = 1.86(Re\, Pr\, \Omega)^{0.33}, \text{if } Re \leq 2100 \qquad (9)$$

$$Nu = 0.023(1 + 6\Omega)Re^{0.8}\, Pr^{0.33}, \text{if } Re > 2100 \qquad (10)$$

Moreover, due to the transport of water vapor through the membrane pores, the non-volatile components accumulate/dilute in the feed/draw channels in proximity of the membrane surface. As a consequence, a concentration gradient between the feed/draw-membrane interface and the bulk of the solution is generated, and a diffusive flow of solutes induced. At steady state, a concentration profile resulting from the convective transport of solutes towards the membrane surface (in the feed channel, or in the opposite direction for the draw channel) and the diffusive flux of retained compounds towards the bulk solution (in the feed channel, or in the opposite direction for the draw channel) is established, as depicted in Fig. 1a. The Nernst film model, which neglects eddy and thermal diffusion, is extensively exploited in the literature[45,46] to evaluate the ratio between the solute concentration at the membrane surface and in the bulk. For the feed and draw channels, the following equations can be written, respectively:

$$x_{s,m,f} = x_{s,b,f} \exp\left(\frac{J_w}{k_{s,f}}\right) \qquad (11)$$

$$x_{s,m,d} = x_{s,b,d} \exp\left(\frac{-J_w}{k_{s,d}}\right) \qquad (12)$$

where $k_{s,f/d} = \frac{D_{s,w}\rho_{f/d}}{\delta_{boundary}}$ is the mass transfer coefficient, being $D_{s,w}, \rho$ and $\delta_{boundary}$ the solute diffusion in water, the density of the solution in the boundary layer, and the thickness of the boundary layer, respectively. A concentrative concentration polarization coefficient can be defined in the feed solution as $\theta_{s,f} = \frac{x_{s,m,f}}{x_{s,b,f}}$. Contrarily, in the draw solution, a dilutive concentration polarization coefficient defined as $\theta_{s,d} = \frac{x_{s,m,d}}{x_{s,b,d}}$ results. Hence, the activity of the solutions at the membrane interfaces is:

$$a(x_{s,m,f}) = a\left(x_{s,b,f} \exp\left(\frac{J_w}{k_{s,f}}\right)\right) \qquad (13)$$

$$a(x_{s,m,d}) = a\left(x_{s,b,d} \exp\left(\frac{-J_w}{k_{s,d}}\right)\right) \qquad (14)$$

It is worth noting that this is valid if the non-volatile components are retained by the membrane, which is the case for the process

under consideration. The activity values of the solutions were calculated from the *Idaho Database of Solution Thermodynamics (IDST)*[28]. To estimate $\delta_{boundary}$, mass transfer empirical correlations were exploited[45]:

$$Sh = 1.62(Re\,Sc\,\Omega)^{0.33}, \text{if } Re \leq 2100 \tag{15}$$

$$Sh = 0.023\,Re^{0.8}\,Sc^{0.33}, \text{if } Re > 2100 \tag{16}$$

where Sh, Sc are the Sherwood and Schmidt numbers, and $\delta_{boundary} = \frac{d_h}{Sh}$.

To summarize, Eq. (4) represents a model that incorporates the heat and mass transfer mechanisms occurring both across the membrane and in the feed and draw channels, where boundary layers are induced by thermofluid-dynamic conditions. Therefore, to accurately determine the effective water vapor flux through the membrane, the polarization phenomena, and consequently the effective concentration and temperature values at the interfaces between the aqueous solutions (both feed and draw) and the membrane, shall be taken into consideration.

Simplified, linearized model

The implicit non-linear Eq. (4) outlines the logarithmic dependence of water vapor flux on its mole fraction, computed at the interface between the aqueous solutions (both feed and draw) and the membrane. Calculating the latter variable requires knowledge of the relationship between activity and molarity of the solution (see Eqs. (13) and (14)) and semi-empirical heat and mass transfer correlations (see Eqs. (9), (10) and Eqs. (15) and (16)) for the boundary layers. Clearly, the implicit nature of Eq. (4) and the need for various correlations imply a number of cumbersome calculations, which may limit the exploitation of this OMD model by the community.

For practical purposes, a streamlined linearized version of Eq. (4) is derived and described below, making it simpler to use, albeit with some necessary approximations. Typically, as a result of the low transmembrane bulk temperature difference, the permeate water vapor flux can be linearly related to its partial pressure difference across the membrane pores:

$$J_w = K\Delta p_v = \left(\frac{1}{\frac{2M_{H_2O}\epsilon_m r}{3RT\delta_m\tau}\sqrt{\frac{8RT}{\pi M_{H_2O}}}} + \frac{1}{\frac{\epsilon_m PD_{w,a}M_{H_2O}}{p_a\tau RT\delta_m}} \right)^{-1} \Delta p_v \tag{17}$$

where K is the permeability coefficient and p_a the arithmetic mean of the partial pressures of air in the pores. Then, in case of diluted conditions, the activity of the solution can be assumed as linearly dependent on the molar fraction of the non-volatile solute[27], namely $a(x_s) = 1 - x_s$, resulting in the following equations for the activity of the solutions:

$$a_{m,f} = 1 - x_{s,m,f} = 1 - x_{s,b,f}\exp\left(\frac{J_w}{k_{s,f}}\right) \tag{18}$$

$$a_{m,d} = 1 - x_{s,m,d} = 1 - x_{s,b,d}\exp\left(\frac{-J_w}{k_{s,d}}\right) \tag{19}$$

Furthermore, as measuring the temperature at the feed and draw sides is more feasible than determining the partial pressure, the water vapor flux can be evaluated using the well-known Clausius-Clapeyron equation[27,46]:

$$\Delta p_v = \frac{dp_v}{dT}\bigg|_{\tilde{T}_m}(T_{m,f} - T_{m,d})(1 - \tilde{x}) + p_v(\tilde{T}_m)\big[(1 - x_{f,m}) - (1 - x_{d,m})\big] \tag{20}$$

where $\frac{dp_v}{dT}\big|_{\tilde{T}_m} = \left(\frac{\Delta H}{RT^2}\right)p_v(\tilde{T})$ represents the variation of vapor pressure at the vapor-water equilibrium interface at constant

temperature. The final linearized expression is therefore written as:

$$J_w = K(\tilde{T})p_v(\tilde{T})\left[\frac{\Delta H(\tilde{T})}{R\tilde{T}^2}\theta_T\Delta T\left(1 - \frac{\theta_{s,d}\,x_{s,b,d} + \theta_{s,f}\,x_{s,b,f}}{2}\right) + (\theta_{s,d}\,x_{s,b,d} - \theta_{s,f}\,x_{s,b,f})\right] \tag{21}$$

Typically, the permeability coefficient K can be easily estimated by experiments. Therefore, with knowledge of the bulk solute mole fractions and temperatures of both feed and draw streams (i.e., $x_{s,b,f}$, $x_{s,b,d}$, $T_{b,f}$, $T_{b,d}$), the water vapor flux through the membrane can be explicitly and easily estimated. This estimation relies on assuming or fitting the temperature and concentration polarization coefficients to experimental data. Indeed, with the knowledge of $T_{b,f}$ and $T_{b,d}$, calculating the values of $\tilde{T}$ and ΔT in Eq. (21) becomes straightforward as well.

REFERENCES

1. Quist-Jensen, C. A., Ali, A., Mondal, S., Macedonio, F. & Drioli, E. A study of membrane distillation and crystallization for lithium recovery from high-concentrated aqueous solutions. *J. Membr. Sci.* **505**, 167–173 (2016).
2. Ali, A. et al. A review of membrane crystallization, forward osmosis and membrane capacitive deionization for liquid mining. *Resour., Conserv. Recycling* **168**, 105273 (2021).
3. Tost, M. et al. Ecosystem services costs of metal mining and pressures on biomes. *Extractive Industries Soc.* **7**, 79–86 (2020).
4. Gryta, M. The long-term studies of osmotic membrane distillation. *Chem. Pap.* **72**, 99–107 (2018).
5. Terki, L. et al. Implementation of osmotic membrane distillation with various hydrophobic porous membranes for concentration of sugars solutions and preservation of the quality of cactus pear juice. *J. Food Eng.* **230**, 28–38 (2018).
6. Ricceri, F. et al. Microalgae biomass concentration and reuse of water as new cultivation medium using ceramic membrane filtration. *Chemosphere* **307**, 135724 (2022).
7. Malaguti, M. et al. Dewatering of scenedesmus obliquus cultivation substrate with microfiltration: potential and challenges for water reuse and effective harvesting. *Engineering* (2023). https://www.sciencedirect.com/science/article/pii/S2095809923003417.
8. Cassano, A. & Drioli, E. Concentration of clarified kiwifruit juice by osmotic distillation. *J. Food Eng.* **79**, 1397–1404 (2007).
9. Bertozzi, E. et al. Concentration of phycocyanin and coffee extracts in aqueous solutions with osmotically-assisted membrane distillation. *Sep. Purif. Technol.* **330**, 125360 (2023).
10. Bologna, A. et al. Techno-economic analysis of a solar thermal plant for large-scale water pasteurization. *Appl. Sci.* **10**, 4771 (2020).
11. Wu, J. et al. Techno-economic comparison between forward osmosis (fo) and temperature-enhanced osmotic membrane distillation (t-omd) in agricultural fertigation. *J. Water Process Eng.* **43**, 102216 (2021).
12. Kujawa, J. et al. Raw juice concentration by osmotic membrane distillation process with hydrophobic polymeric membranes. *Food Bioprocess Technol.* **8**, 2146–2158 (2015).
13. Ahmad, S. et al. Mass transfer modelling of hollow fiber membrane contactor for apple juice concentration using osmotic membrane distillation. *Sep. Purif. Technol.* **250**, 117209 (2020).
14. Zhang, Z. et al. The role of osmotic agent in water flux enhancement during osmotic membrane distillation (omd) for treatment of highly saline brines. *Desalination* **481**, 114353 (2020).
15. Wang, L. & Min, J. Modeling and analyses of membrane osmotic distillation using non-equilibrium thermodynamics. *J. Membr. Sci.* **378**, 462–470 (2011).

16. Volpin, F. et al. Simultaneous phosphorous and nitrogen recovery from source-separated urine: a novel application for fertiliser drawn forward osmosis. *Chemosphere* **203**, 482–489 (2018).

17. Giagnorio, M. et al. Coupling of forward osmosis with desalination technologies: system-scale analysis at the water-energy nexus. *Desalination* **543**, 116083 (2022).

18. Rehman, W. U., Muhammad, A., Khan, Q. A., Younas, M. & Rezakazemi, M. Pomegranate juice concentration using osmotic distillation with membrane contactor. *Sep. Purif. Technol.* **224**, 481–489 (2019).

19. Alves, V. & Coelhoso, I. Study of mass and heat transfer in the osmotic evaporation process using hollow fibre membrane contactors. *J. Membr. Sci.* **289**, 249–257 (2007).

20. Bagci, P. O., Akbas, M., Gulec, H. A. & Bagci, U. Coupling reverse osmosis and osmotic distillation for clarified pomegranate juice concentration: Use of plasma modified reverse osmosis membranes for improved performance. *Innovative Food Sci. Emerg. Technol.* **52**, 213–220 (2019).

21. Rehman, W.-U. et al. Effect of membrane wetting on the performance of pvdf and ptfe membranes in the concentration of pomegranate juice through osmotic distillation. *J. Membr. Sci.* **584**, 66–78 (2019).

22. Ma, Z. et al. Selective and high-efficient removal of tetracycline from antibiotic-containing aqueous solution via membrane adsorption with membrane pre-concentration. *J. Water Process Eng.* **50**, 103281 (2022).

23. Ullah, S. Z. et al. Cfd simulation of osmotic membrane distillation using hollow fiber membrane contactor: operating conditions and concentration polarization effects. *Chem. Eng. Res. Des.* **197**, 984–996 (2023).

24. Babu, B. R., Rastogi, N. & Raghavarao, K. Concentration and temperature polarization effects during osmotic membrane distillation. *J. Membr. Sci.* **322**, 146–153 (2008).

25. Babu, B. R., Rastogi, N. & Raghavarao, K. Mass transfer in osmotic membrane distillation of phycocyanin colorant and sweet-lime juice. *J. Membr. Sci.* **272**, 58–69 (2006).

26. Ahmad, S. et al. Development of mass and heat transfer coupled model of hollow fiber membrane for salt recovery from brine via osmotic membrane distillation. *Environ. Sci. Eur.* **33**, 1–18 (2021).

27. Khayet, M., Souhaimi, M. K. & Matsuura, T. Membrane distillation: principles and applications (2011). https://www.sciencedirect.com/book/9780444531261/membrane-distillation.

28. Robinson, R. A. & Stokes, R. H. *Electrolyte Solutions* (Courier Corporation, 2002).

29. Ricceri, F. et al. Desalination of produced water by membrane distillation: Effect of the feed components and of a pre-treatment by fenton oxidation. *Sci. Rep.* **9**, 14964 (2019).

30. Mengual, J. I., Pen, L. & Vela, A. et al. Osmotic distillation through porous hydrophobic membranes. *J. Membr. Sci.* **82**, 129–140 (1993).

31. Courel, M., Dornier, M., Herry, J.-M., Rios, G. M. & Reynes, M. Effect of operating conditions on water transport during the concentration of sucrose solutions by osmotic distillation. *J. Membr. Sci.* **170**, 281–289 (2000).

32. El-Abbassi, A., Khayet, M., Kiai, H., Hafidi, A. & García-Payo, Md. C. Treatment of crude olive mill wastewaters by osmotic distillation and osmotic membrane distillation. *Sep. Purif. Technol.* **104**, 327–332 (2013).

33. Nagaraj, N. et al. Mass transfer in osmotic membrane distillation. *J. Membr. Sci.* **268**, 48–56 (2006).

34. Shah, K. M. et al. Drivers, challenges, and emerging technologies for desalination of high-salinity brines: a critical review. *Desalination* **538**, 115827 (2022).

35. Alberghini, M. et al. Multistage and passive cooling process driven by salinity difference. *Sci. Adv.* **6**, eaax5015 (2020).

36. Ricceri, F. et al. Unraveling the role of feed temperature and cross-flow velocity on organic fouling in membrane distillation using response surface methodology. *Desalination* **540**, 115971 (2022).

37. Chiavazzo, E., Morciano, M., Viglino, F., Fasano, M. & Asinari, P. Passive solar high-yield seawater desalination by modular and low-cost distillation. *Nat. Sustain.* **1**, 763–772 (2018).

38. Antonetto, G. et al. Synergistic freshwater and electricity production using passive membrane distillation and waste heat recovered from camouflaged photovoltaic modules. *J. Clean. Prod.* **318**, 128464 (2021).

39. Deshmukh, A. & Elimelech, M. Understanding the impact of membrane properties and transport phenomena on the energetic performance of membrane distillation desalination. *J. Membr. Sci.* **539**, 458–474 (2017).

40. Lee, J., Straub, A. P. & Elimelech, M. Vapor-gap membranes for highly selective osmotically driven desalination. *J. Membr. Sci.* **555**, 407–417 (2018).

41. Deshmukh, A. et al. Membrane distillation at the water-energy nexus: limits, opportunities, and challenges. *Energy Environ. Sci.* **11**, 1177–1196 (2018).

42. Mackie, J. & Meares, P. The diffusion of electrolytes in a cation-exchange resin membrane i. theoretical. *Proc. R. Soc. Lond. Ser. A. Math. Phys. Sci.* **232**, 498–509 (1955).

43. Srisurichan, S., Jiraratananon, R. & Fane, A. Mass transfer mechanisms and transport resistances in direct contact membrane distillation process. *J. Membr. Sci.* **277**, 186–194 (2006).

44. Alberghini, M. et al. Textured and rigid capillary materials for passive energy-conversion devices. *Adv. Mater. Interfaces* **9**, 2200057 (2022).

45. Alkhudhiri, A., Darwish, N. & Hilal, N. Membrane distillation: a comprehensive review. *Desalination* **287**, 2–18 (2012).

46. Kim, A. S. A two-interface transport model with pore-size distribution for predicting the performance of direct contact membrane distillation (dcmd). *J. Membr. Sci.* **428**, 410–424 (2013).

ACKNOWLEDGEMENTS

AUTHOR CONTRIBUTIONS

A.T. conceived the idea of the study. M.F. and A.T. found financial support and supervised the research activities. M.Mo. and M.F. developed the model; M.Mo. performed all the calculations. M.Ma. and F.R. performed all the experiments supported by A.T. All authors helped with the result presentation and interpretation. M.Mo. and M.Ma. wrote the first draft of the article; all authors contributed to the final paper writing.

COMPETING INTERESTS

The authors declare no competing interests.

ADDITIONAL INFORMATION

Supplementary information The online version contains supplementary material available at https://doi.org/10.1038/s41545-023-00294-2.

Correspondence and requests for materials should be addressed to Alberto Tiraferri or Matteo Fasano.

Reprints and permission information is available at http://www.nature.com/reprints

Publisher's note Springer Nature remains neutral with regard to jurisdictional claims in published maps and institutional affiliations.